

Cardiac Strain Imaging With Coherent Compounding of Diverging Waves

Julien Grondin, Vincent Ssayseng, and Elisa E. Konofagou, *Member, IEEE*

Abstract—Current methods of cardiac strain imaging at high frame rate suffer from motion matching artifacts or poor lateral resolution. Coherent compounding has been shown to improve echocardiographic image quality while maintaining a high frame rate, but has never been used to image cardiac strain. However, myocardial velocity can have an impact on coherent compounding due to displacements between frames. The objective of this paper was to investigate the feasibility and performance of coherent compounding for cardiac strain imaging at a low and a high myocardial velocity. Left-ventricular contraction in short-axis view was modeled as an annulus with radial thickening and circumferential rotation. Simulated radio-frequency channel data with a cardiac phased array were obtained using three different beamforming methods: single diverging wave, coherent compounding of diverging waves, and conventional focusing. Axial and lateral displacements and strains as well as radial strains were estimated and compared to their true value. *In vivo* feasibility of cardiac strain imaging with coherent compounding was performed and compared to single diverging wave imaging. At low myocardial velocities, the axial, lateral, and radial strain relative error for nine compounded waves (16.3%, 40.4%, and 18.9%) were significantly lower than those obtained with single diverging wave imaging (19.9%, 80.3%, and 30.6%) and closer to that obtained with conventional focusing (16.7%, 43.7%, and 16%). *In vivo* left-ventricular radial strains exhibited higher quality with nine compounded waves than with single diverging wave imaging. These results indicate that cardiac strain can be imaged using coherent compounding of diverging waves with a better performance than with single diverging wave imaging while maintaining a high frame rate, and therefore, has the potential to improve diagnosis of myocardial strain-based cardiac diseases.

Index Terms—Cardiac strain imaging, coherent compounding, high frame rate imaging, ultrasound simulation.

I. INTRODUCTION

CARDIAC strain imaging with ultrasound can be used for the detection and characterization of myocardial contraction abnormalities [1], [2]. The quality of cardiac strain estimation can be increased using frame rates higher than those achieved by conventional imaging due to lower signal decorrelation [3]. Previous studies have shown that a higher frame rate can be achieved with methods such as multiline acquisition

[4], [5], multiline transmit [6], [7], or ECG-gated acquisitions [8]. Multiline transmit is prone to crosstalk artifacts and ecg-gated acquisitions can produce breathing or inconsistent heartbeats artifacts. Ultrafast imaging has been introduced to image the entire field of view with a single plane wave at high temporal resolution [9]. However, although plane wave imaging can be performed in the heart [10], its field of view can be limited by the transducer aperture, which cannot always include the entire heart for all the standard echocardiographic views. Therefore, diverging wave imaging has been developed for cardiac imaging by placing a virtual source behind the transducer to image the heart with a single transmitted beam at high temporal resolution [11]–[13]. However, the use of a single unfocused transmitted beam to reconstruct an image affects the quality of the image such as the contrast, the signal-to-noise ratio (SNR), and the lateral resolution. In order to compensate those effects, coherent compounding of unfocused beams has been introduced. Montaldo *et al.* [14] have shown that coherent compounding of plane waves at different angles can provide echographic images with a quality as good as those obtained with multifocus imaging while maintaining a high frame rate. In addition to improvements in B-mode image quality, coherent compounding has also been shown to improve cardiovascular strain images. Korukonda *et al.* [15] have investigated the performance of sparse-array, plane wave, and compounded plane wave imaging for vascular elastography *in silico*, in phantoms, and *in vivo* with a linear array transducer. They showed that sparse-array imaging yielded reduced sidelobes compared to single and compounded plane wave imaging, but the latter produced visually better vascular elastograms *in vivo*. More recently, Porée *et al.* [16] have shown that coherent compounding of plane waves can increase the quality of vascular strain images compared to conventional focusing. However, the heart is a fast-moving organ with higher motion amplitudes and that is imaged with phased arrays, which, generally, has a lower center frequency and smaller aperture than linear arrays used for vascular imaging. Therefore, for clinical cardiovascular imaging, phased arrays are expected to have a lower lateral resolution than linear arrays, according to the formula for full-width half-maximum (FWHM) [17], i.e.,

$$\text{FWHM} = 1.4 \frac{\lambda F}{A} \quad (1)$$

where λ is the wavelength, F is the focal depth, and A is the aperture. Therefore, the benefit of coherent compounding for cardiac strain imaging with a phased array had to be investigated separately.

Coherent compounding of diverging waves has been used for cardiac imaging by moving the virtual source later-

Manuscript received December 19, 2016; accepted June 16, 2017. Date of publication June 20, 2017; date of current version August 4, 2017. This work was supported by the National Institutes of Health under Grant R01-EB006042. (Corresponding author: Elisa E. Konofagou.)

J. Grondin and V. Ssayseng are with the Department of Biomedical Engineering, Columbia University, New York, NY 10027 USA (e-mail: jlg2216@columbia.edu).

E. E. Konofagou is with the Department of Biomedical Engineering, Columbia University, New York, NY 10027 USA, and also with the Department of Radiology, Columbia University, New York, NY 10032 USA (e-mail: ek2191@columbia.edu).

Digital Object Identifier 10.1109/TUFFC.2017.2717792

ally for different acquisitions using methods similar to the previously developed synthetic transmit aperture [18]. Papadacci *et al.* [12] have shown that spatially coherent compounded diverging waves at high frame rates improved the SNR of cardiac images *in vivo* as well as the quality of tissue velocity images compared to a single diverging wave. Nillesen *et al.* [19] have shown the feasibility of coherent compounding of five diverging waves for 2-D cardiac motion estimation in a simulation study. However, tissue motion between consecutive transmits can affect image quality during coherent compounding. In a recent study, Porée *et al.* [20] integrated motion compensation to coherent compounding of diverging waves to obtain high-contrast echocardiographic B-mode and tissue Doppler images. However, to our knowledge, no study has investigated myocardial strain imaging with coherent compounding as of yet.

Our objective was to investigate the performance of coherent compounding of diverging waves in 2-D cardiac strain imaging. First, the effect of the number of compounded waves, using subapertures, on the quality of the motion and strain estimation was investigated in a cardiac numerical phantom. Then, the performance of the optimal number of compounded waves was compared to that obtained with a single diverging wave using full aperture and with conventional focused beams. Finally, *in vivo* feasibility of cardiac strain imaging using coherent compounding was performed on a healthy volunteer.

II. METHODS

A. Point-Spread Function

The performance of each beamforming method described in Section II-B was investigated by characterizing the lateral point spread function (PSF). A phantom with a single scatterer at a depth of 45 mm and centered laterally was simulated with Field II and the B-mode images were generated after enveloped detection and logarithmic compression of the coherently compounded diverging waves. The lateral profile of the B-mode images at 45 mm depth were then obtained for $N = 1$ to 51 compounded waves as well as for single diverging with full aperture and for conventional focusing.

B. Phantom Design

The parasternal short-axis view of the left ventricle was modeled as an annulus with an outer diameter of 50 mm and a wall thickness of 10 mm (Fig. 1). Previous studies have also used an annular shape to represent the left ventricle in short axis view [21], [22] or the cross section of the carotid artery [15], [16]. The size of the annulus was chosen according to the left ventricle diameter reported in [23]. The center of the annulus was located at 45 mm from the surface of the transducer and centered laterally. Myocardial contraction is a dynamic phenomenon during which myocardial velocity varies and can differ among subjects. Myocardial contraction in the short-axis view was modeled as an inward radial motion with a linear gradient from the outer boundary (i.e., epicardium) of the phantom with no radial motion to the inner boundary (i.e., endocardium) with a radial velocity of 2.1 cm/s (34.1 wavelengths/s) or 21 cm/s (341 wavelengths/s), which would span

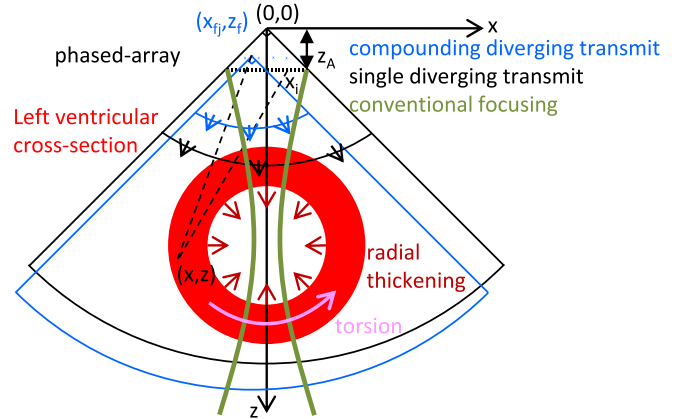


Fig. 1. Schematic of the left-ventricular phantom and the simulation configuration. The left-ventricle is modeled as an annulus with an increasing radial motion from the outer to the inner boundary. Myocardial torsion is modeled by a homogeneous circumferential motion. Three different beamforming methods were investigated separately and represented here in different colors. For single diverging wave imaging (in black), a single virtual source is placed at $(0,0)$ with an angle of aperture of 90° . For coherent compounding of diverging waves, $N = 5$ virtual sources are represented (in blue) at (x_{ij}, z_{ij}) . The trajectory corresponding of the time of flight from the virtual source to a point (x, z) of the phantom and back to an element x_i of the phased array is represented (in a dotted black line). For conventional focusing, the center emission is represented (in green).

the range of normal average myocardial velocities [24]. The imaging depth was 11 cm, which allows a maximum pulse repetition frequency (PRF) of 7 kHz. The contraction of the phantom was modeled only for the time needed to acquire two frames for each beamforming technique. Torsion of the heart was modeled by simulating a rotation of the annulus using a physiologic twisting rate of $70^\circ/\text{s}$ [25] at a myocardial velocity of 21 cm/s. The twisting rate was proportionally adjusted to the myocardial velocity. The radial motion corresponding to contraction and the circumferential motion associated with torsion were combined to simulate left ventricular contraction. A simulation with no myocardial motion between transmitted pulses, but with a myocardial velocity of 21 cm/s between compounded frames was also performed to investigate the intrinsic effect of coherent compounding on strain estimation regardless of myocardial motion between transmitted pulses.

C. Simulation Design

The program Field II was used to generate the ultrasound radio-frequency (RF) channel data from a simulated transducer and a scatterers distribution [26]. The number of scatterers was superior to 10 per resolution cell in order to generate a fully developed speckle [27]. The scatterers had uniformly distributed random positions and normally distributed random amplitudes. The scattering amplitude was ten times higher in the annulus than in the background medium. The scatterers in the background medium were static over time. In this study, the ATL P4-2 cardiac probe with $N_A = 64$ elements, 20.5-mm full aperture, $f_c = 2.5$ MHz center frequency was simulated with 60% bandwidth at -6 dB and we investigate three different beamforming methods for cardiac strain imaging. Although previous studies modeled carotid cross section as an annulus and investigated the quality of the strain images using

different beamforming techniques such as sparse-array imaging, coherent plane wave imaging, and conventional focusing using a linear array [15], [16], they differ from this study in that a phased array was used for myocardial imaging.

In this study, for the first imaging method, single diverging wave imaging using the full aperture was simulated by placing a virtual source behind the transducer at a distance (z_A) equal to half of the full aperture and centered laterally in order to insonify the medium with a 90° angle. A standard delay-and-sum algorithm was used to reconstruct the image on a polar grid of 128 lines on a 90° field of view and an imaging depth of 85 mm with an axial sampling of 0.0385 mm.

In the second imaging method, coherent compounding of diverging waves was performed using a subaperture of $N_{SA} = 21$ elements in emission as in [12] and [19]. However, full aperture was used in receive. The number (N) of diverging waves to reconstruct one image was 1, 3, 5, 9, 15, 21, or 51. For $N = 1$, the virtual subaperture source was centered laterally and placed at a distance equal to half the size of the subaperture behind the surface of the transducer to obtain a 90° angle aperture. For $N \geq 3$, the lateral position of the virtual sources was spaced evenly between the 11th and the 54th element with the same axial position as for $N = 1$. In this configuration, a large virtual aperture, obtained by a large virtual pitch or a large number of transmits, would increase the lateral resolution, but a large virtual pitch would also increase the grating lobes [12]. Therefore, a small transmit subaperture increases the virtual subaperture and subsequently improves the lateral resolution but decreases the transmitted pressure. Consequently, the quality of the images and of the displacement and strains depends on these parameters and a subaperture of 21 elements was found to be a good tradeoff [12].

The quality of the strain images depends on the magnitude of the interframe displacement and strain [3], [28]. Increasing the number of diverging waves from $N = 1$ to 51 will increase the magnitude of the estimated displacement due to motion between transmitted diverging waves. Therefore, the intrinsic effects of coherent compounding and of increased displacement magnitude on displacement estimation quality are not independent. In order to isolate the effect of coherent compounding from that of interframe displacements, a set of simulations with $N = 1$ was performed for the interframe displacement corresponding to $N = 3$ to 51 at both low and high myocardial velocities. For each emission with a diverging wave using subapertures, the image was reconstructed on the same polar grid as for the single diverging wave using full aperture. The time of flight between the emission from the virtual source and the reception on all the elements was computed as follows:

$$T_f = T_t + T_r - T_d \quad (2)$$

where

$$T_t = \frac{\sqrt{(x_{fj} - x)^2 + (z_f - z)^2}}{c} \quad (3)$$

denotes the time of flight from a virtual focus (x_{fj}, z_f) to a point of the grid (x, z), and c is the speed of sound, assumed

to be 1540 m/s. For single diverging wave imaging with full aperture, $x_{fj} = z_f = 0$

$$T_r = \frac{\sqrt{(x_i - x)^2 + (z_A - z)^2}}{c} \quad (4)$$

is the time of flight from the point of the grid (x, z) to the i th element of the transducer (x_i, z_A), and

$$T_d = \frac{z_A - z_f}{c} \quad (5)$$

is the time that must be removed from T_f to take into account the virtual propagation from the source to the first element to emit. For each value of N , the reconstructed RF signals were added together over each emission to obtain a coherently compounded image.

In the third imaging method, conventional focusing was used with 128 beams steering across 90° , with a transmit focus at 45 mm. For each focused transmit, a standard delay-and-sum algorithm was used to reconstruct the corresponding line with the same axial sampling as in the aforementioned imaging methods in order to achieve dynamic receive focusing. The interframe displacements of the inner boundary of the phantom for conventional focusing using 128 beams for a PRF of 7 kHz and myocardial velocities of 2.1 and 21 cm/s are 384 and 3.84 mm, respectively. Therefore, the comparison between the different beamforming methods was performed for the same interframe displacement of 384 and 3.84 mm for low and high myocardial velocities, respectively.

For each imaging method, randomly generated Gaussian noise was added to the RF channel data in order to simulate electronic noise and obtain ultrasound images with a SNR of 15 dB for the single diverging wave method, similar to what was obtained *in vivo*. The SNR was defined *in vivo* as 10 times the logarithm of the root-mean-square (RMS) power of the signal in the myocardium relative to the RMS power of the myocardial cavity.

D. Effect of SNR and Background Medium Level

Although coherent compounding has been shown to improve B-mode image quality, strain estimation accuracy may be significantly impacted if the image quality such as SNR or contrast is too poor. Therefore, the effect of SNR and of the amplitude of the background medium was investigated in the simulation configuration with $N = 9$ compounded diverging. In one case, the ratio of scattering amplitude of the annulus over that of the background medium was kept at 10 and the SNR for $N = 9$ ranged from 5 to 25 dB by varying the amplitude of the electronic noise and the radial strain error was computed for each value of the SNR. In the other case, the electronic noise added to the channel data was set to obtain a SNR of 15 dB for the single diverging wave method and the ratio of scattering amplitude of the annulus over that of the background medium ranged from 1.5 to 20 and the radial strain error was computed for each ratio.

E. Motion and Strain Estimation

Axial and lateral displacements, which refer to displacements in the direction of propagation of the wave and the direction perpendicular to the axial direction in the imaging plane,

respectively, were estimated using normalized 1-D (axial) cross correlation of the reconstructed RF signals in a 2-D (axial and lateral) search with a window size of 3.1 mm, 70% overlap and a 30:1 linear interpolation scheme between adjacent RF signals [29]. A recorrelation method was used to improve the lateral motion estimation by correcting for the axial motion as described in [29]. Briefly, the RF signals are axially shifted in the second frame by an amount equal to the opposite of the estimated axial displacement. Axial and lateral displacements are estimated for a second time between the RF signals in the first frame and the corrected RF signals in the second frame. Three iterations of the 2-D motion estimation were sufficient to reach a steady correlation coefficient and estimation of lateral displacement. The final axial motion was obtained from the first iteration while the final lateral motion was obtained from the third iteration. A $5 \text{ mm} \times 5^\circ$ median filter was used for smoothing of the axial and lateral displacement images. The 2-D Lagrangian strain tensor was calculated by applying a least-squares estimator implemented with Savitzky-Golay filters [30] on the axial and lateral displacements [29]. The corresponding 1-D kernel was applied both in the axial and the lateral direction to obtain normal and shear strain components. The strain tensor and the axial and lateral displacements were converted from a polar to a Cartesian coordinate system. In the results and discussion sections, axial and lateral displacements and strains are expressed in the Cartesian coordinate system. Finally, radial and circumferential strains, with the origin of the coordinate system at the centroid of the annulus, were obtained from the 2-D strain tensor.

F. In Vivo Feasibility

The parasternal short-axis view of the heart at the mid-level of a healthy volunteer was imaged using a Verasonics system (Vantage 256, Verasonics, Kirkland, WA) and a P4-2 cardiac phased array. An interleaved sequence alternating single diverging wave transmit with full aperture and $N = 9$ diverging waves with subaperture for compounding, similar to those used in the simulations, was used in order to image the same myocardial contraction event with the same frame rate. The PRF was 7 kHz, resulting in an imaging frame rate of 700 Hz for both beamforming methods. Image reconstruction was performed similar to that described for the simulation. The left ventricle was manually segmented on the reconstructed B-mode image. The axial and lateral displacements were estimated with the same method as described in the previous section but using the following parameters: 6.5-mm window length, 95 % overlap, and 10:1 interpolation factor. Interframe radial strains were obtained similarly as in the previous section and were accumulated during systole for both imaging sequences.

G. Data Analysis

For each number of diverging waves used for compounding and each beamforming method, the axial, lateral and radial strain errors as well as the correlation coefficient were

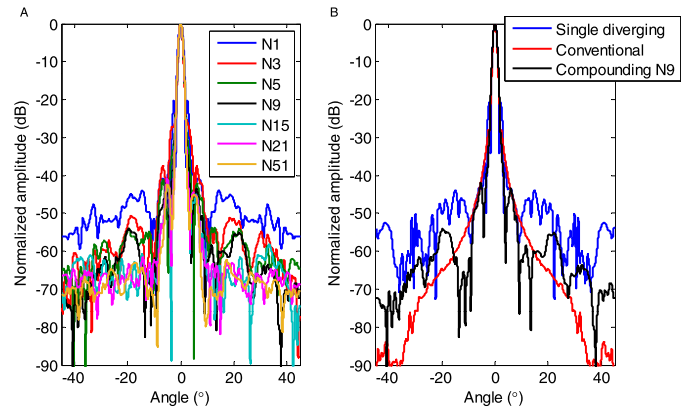


Fig. 2. Lateral PSF (A) for $N = 1$ to 51 coherently compounded diverging waves as well as (B) for each beamforming techniques. For coherent compounding, the full-width half-maximum ranged between 1.6 and 1.9 mm and the level of the secondary lobes decreased when the number of compounded waves increased. Coherent compounding of $N = 9$ diverging waves exhibited a lateral PSF between that obtained for conventional focusing and for single diverging wave with full aperture.

computed. Strain error was computed as

$$\text{Error}(\%) = \frac{\sum_{i=1}^P |\text{ES} - \text{TS}|}{\sum_{i=1}^P |\text{TS}|} \times 100 \quad (6)$$

where ES is the estimated strain image, TS is the true strain image, and P is the number of pixels in the annulus. True axial, lateral, and radial strain images were obtained using the same method as in the previous section from the input axial and lateral displacements used for the contraction of the annulus. The mean correlation coefficient inside the annulus was also computed for each case. For the *in vivo* experiment, the end-systolic elastographic SNR (SNRe), defined as the ratio between the mean and the standard deviation of the end-systolic radial strain, was calculated.

III. RESULTS

A. Comparison of the Number of Diverging Waves

The lateral PSF for coherent compounding of $N = 1$ to 51 diverging waves was characterized [Fig. 2(A)]. The lateral PSF was for each number compounded waves overlapped above -20 dB. The full-width half-maximum at -6 dB ranged between 1.6 and 1.9 mm. Below -20 dB, the level of secondary lobes decreased when the number of compounded waves increased. The change in the lateral PSF as a function of the number of compounded waves was marginal for $N > 9-15$ compared to when $1 \leq N \leq 5$.

The axial, lateral, and radial strain estimation errors as well as the mean correlation coefficient are shown as a function of the number of diverging waves with $N = 1, 3, 5, 9, 15, 21,$ and 51 for a myocardial velocity of 21 cm/s with no motion between pulses (Fig. 3). The axial, lateral, and radial strain estimation errors decrease rapidly from $N = 1$ to 9 and continue to decrease slowly from $N = 9$ to 51 diverging waves. The correlation coefficient always increases with the number of diverging waves.

Performance of coherent compounding was also investigated at low and high myocardial velocities. Axial and lateral

Performance of coherent compounding with no motion between diverging transmits

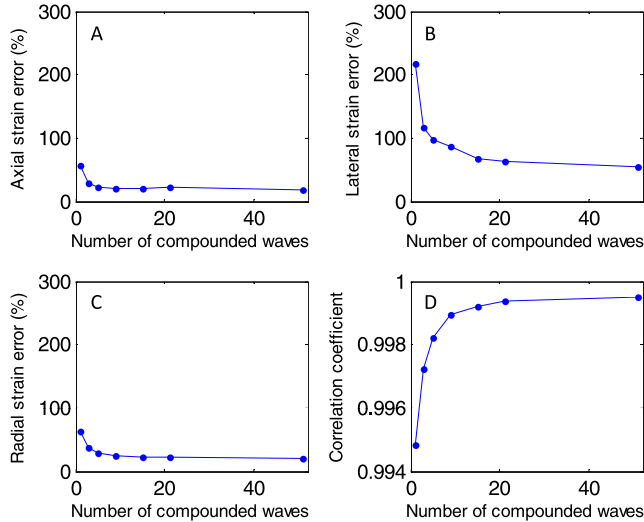


Fig. 3. (A) Axial, (B) lateral, and (C) radial strain error as a function of the number of compounded diverging waves with no motion between diverging transmits. (D) Mean correlation coefficient inside the phantom is also shown. Strain accuracy and correlation coefficient are improved as the number of compounded waves increases from 1 to 51.

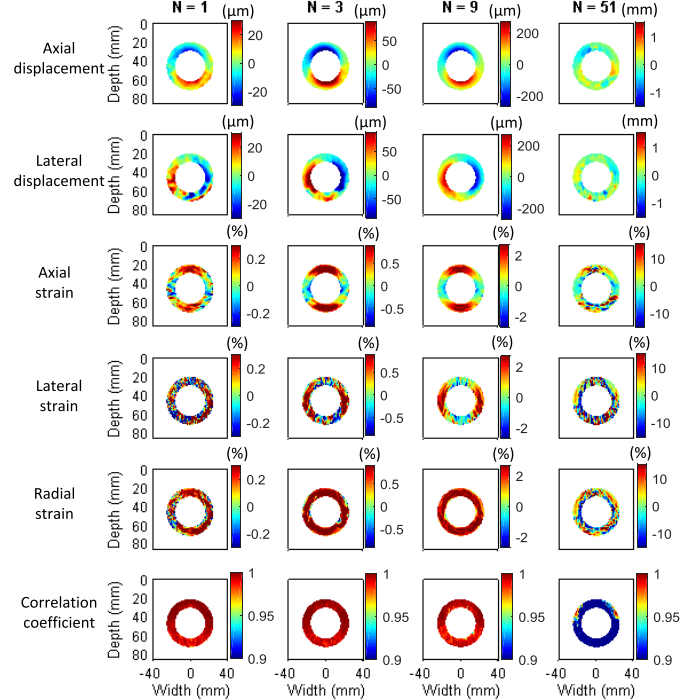
Coherent compounding of N diverging waves for a myocardial velocity of 21 cm/s

Fig. 5. Axial and lateral displacements and strains as well as radial strains and correlation coefficient in the phantom for $N = 1, 3, 9,$ and 51 compounded diverging waves at a myocardial velocity of 21 cm/s. The quality of the estimated displacements and strains increases when N increases and then decreases when for higher N .

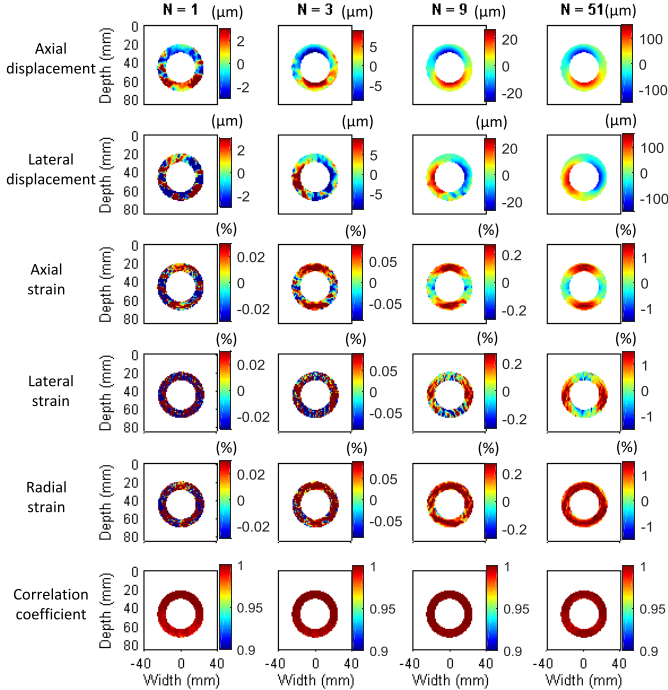
Coherent compounding of N diverging waves for a myocardial velocity of 2.1 cm/s

Fig. 4. Axial and lateral displacements and strains as well as radial strains and correlation coefficient in the phantom for $N = 1, 3, 9,$ and 51 compounded diverging waves at a myocardial velocity of 2.1 cm/s. The quality of the estimated displacements and strains increases when N increases.

displacements and strains as well as radial strains and the correlation coefficient obtained with coherent compounding using a number of diverging waves $N = 1, 3, 9,$ and 51 with a myocardial velocity of 2.1 cm/s are shown in Fig. 4. Positive axial displacements in red tones indicate motion toward the transducers and negative axial displacements in blue tones

indicate motion away from the transducer. Positive lateral displacements in red tones indicate motion to the right and negative lateral displacements in blue tones indicates motion to the left. Axial and lateral displacement images show inward motion of the annulus. Positive strains in red tones indicate lengthening and negative strains in blue tones indicate shortening. The quality of axial displacement and strain images is higher than that of lateral displacement and strain images, respectively. As the number of transmits increases, the quality of the axial and lateral displacement and strain increases and the radial strain becomes more homogeneous. The comparison of axial and lateral displacements and strains as well as radial strains and the correlation coefficient obtained with coherent compounding using a number of diverging waves $N = 1, 3, 9,$ and 51 was also performed with a myocardial velocity of 21 cm/s (Fig. 5). As the number of transmits increases from $N = 1$ to 9, the quality of the displacements and strains increases but gets worse for $N = 51$.

The axial, lateral, and radial strain estimation errors as well as the mean correlation coefficient are shown as a function of the number of diverging waves with $N = 1, 3, 5, 9, 15, 21,$ and 51 at a myocardial velocity of 2.1 cm/s (Fig. 6). Quantitative analysis showed that the axial, lateral, and radial strain estimation errors rapidly decreased from $N = 1$ to 9 and continued to decrease slowly from $N = 9$ to 51 diverging waves. Strain estimation errors for single diverging wave imaging for the corresponding interframe displacements follow a similar trend, but are higher than that with coherent compounding. For coherent compounding, the correlation coefficient increases

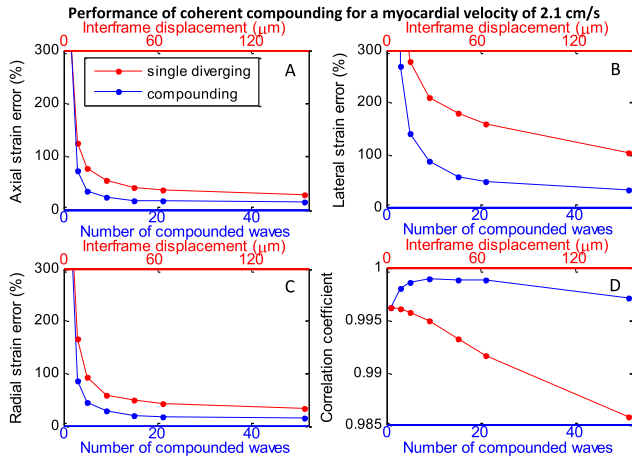


Fig. 6. (A) Axial, (B) lateral, and (C) radial strain error as a function of the number of compounded waves at low (2.1 cm/s) myocardial velocities (in blue) as well as single diverging wave imaging ($N = 1$) for the same interframe displacement (in red). (D) Mean correlation coefficient inside the phantom is also shown. Strain accuracy is improved as the number of compounded waves increases from 1 to 51 and as the interframe displacement increases but better strain estimation is obtained with coherent compounding than with single diverging wave imaging.

from $N = 1$ to 9 and then decreases whereas for single diverging wave imaging it monotonously decreases. The axial strain estimation error decreases from 407.5% for $N = 1$ to 15.2% for $N = 51$ and is 23.5% when $N = 9$. The lateral strain estimation error decreases from 1486% for $N = 1$ to 33% for $N = 51$ and is 87.9% when $N = 9$. The radial strain estimation error decreases from 467.1% for $N = 1$ to 14.3% for $N = 51$ and is 27.8% when $N = 9$. The mean correlation coefficient increases from 0.9963 for $N = 1$ to 0.9990 for $N = 9$ and then decreases to 0.9972 when $N = 9$.

However, at high wall velocities (21 cm/s), although the axial, lateral, and radial strain estimation errors start to decrease from $N = 1$ to 9, they increase when N is superior to 9 (Fig. 7). A similar trend is also observed in strain estimation errors for single diverging wave imaging for the corresponding interframe displacements, but with higher errors than with coherent compounding. The axial strain estimation error is 57.5% for $N = 1$, 15% for $N = 9$, and 95.1% for $N = 51$. The lateral strain estimation error is 217.5% for $N = 1$, 41.3% for $N = 9$, and 183.3% for $N = 51$. The radial strain estimation error is 63.8% for $N = 1$, 17.4% for $N = 9$, and 97.8% for $N = 51$. The mean correlation coefficient decreases from 0.9948 for $N = 1$ to 0.6245 for $N = 51$ and is 0.9916 when $N = 9$.

The effect of the SNR and the background medium level on radial strain estimation error is shown in Fig. 8. Radial strain error rapidly decreases from a SNR of 5 to 15 dB and then reaches a plateau. A similar effect is observed with the background medium level: a rapid decrease of the radial strain estimation error is observed within a range of phantom-to-background ratio of 1.5 to 5 and then a plateau is reached.

B. Comparison of the Beamforming Methods

The lateral PSF for each beamforming method was characterized [Fig. 2(B)]. The full-width half-maximum at -6 dB

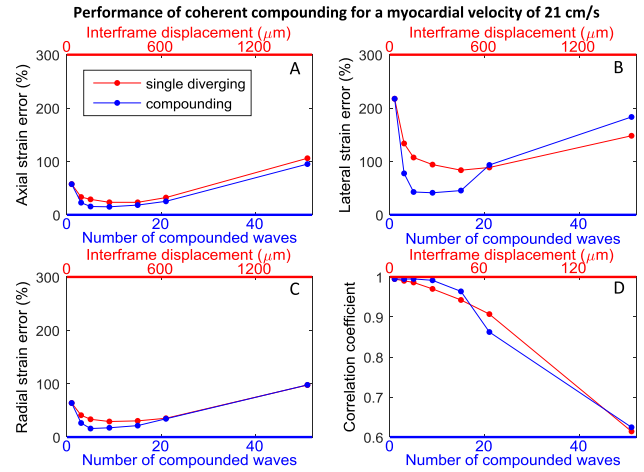


Fig. 7. (A) Axial, (B) lateral, and (C) radial strain error as a function of the number of compounded waves at high (21 cm/s) myocardial velocities (in red) as well as single diverging wave imaging ($N = 1$) for the same interframe displacement (in red). (D) Mean correlation coefficient inside the phantom is also shown. Strain accuracy is improved from 1 to 9 compounded waves and then degrades as the number of compounded waves continues to increase and as the interframe displacement becomes higher. Better strain estimation is obtained with coherent compounding than with single diverging wave imaging.

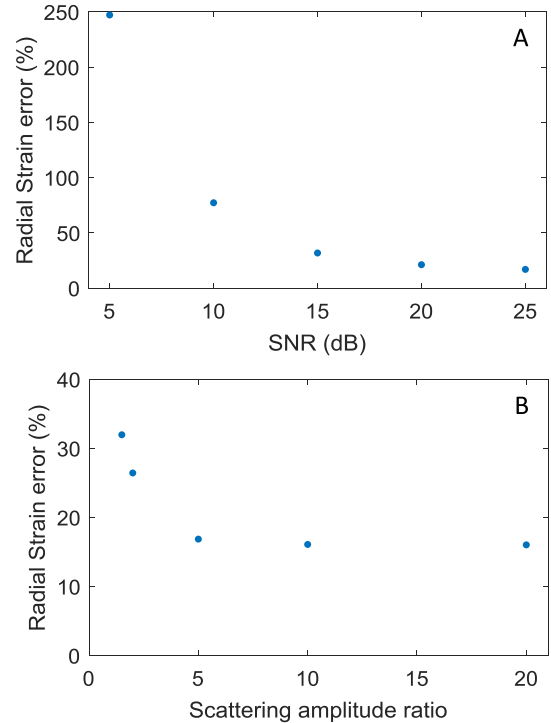


Fig. 8. Radial strain error as a function of (A) SNR and (B) amplitude scattering ratio between the phantom and the background medium for $N = 9$ compounded waves. The radial strain error decreases significantly up to (A) 15 dB and to a ratio of (B) 5 and then reaches a plateau.

was 1.9 mm for single diverging wave with full aperture, 1.7 mm for coherent compounding with $N = 9$ and 1.4 mm for conventional focusing. At 10 mm laterally from the center axis, the amplitude was -33.5 dB for single diverging wave with full aperture, -56.6 dB for $N = 9$ and -71.2 dB for conventional focusing. Coherent compounding of $N = 9$

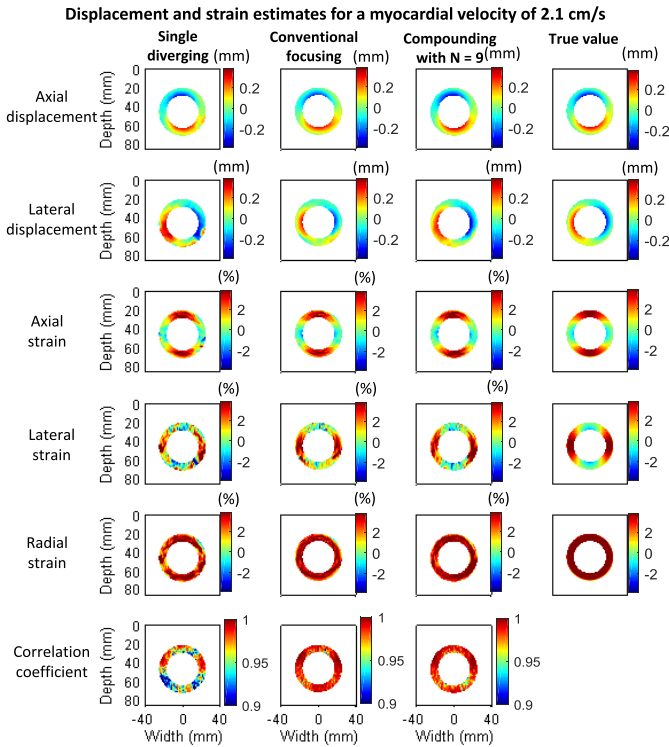


Fig. 9. Axial and lateral displacements and strains as well as radial strains and correlation coefficient in the phantom for single diverging wave imaging, conventional focusing, coherent compounding of $N = 9$ diverging waves and their true value, for an interframe displacement of $384 \mu\text{m}$. The estimated displacements and strains for coherent compounding are better than for single diverging wave and similar to those obtained for conventional focusing.

diverging waves exhibited a lateral PSF more similar to that obtained for conventional focusing than for single diverging wave with full aperture.

The different beamforming methods were compared and $N = 9$ was chosen for the coherent compounding method as it can achieve high frame rate while maintaining a strain estimation accuracy close to that obtained using a higher number of compounded waves at low myocardial velocities and provided a good compromise at high myocardial velocities. Axial and lateral displacements and strains as well as radial strains and correlation coefficient were obtained with single diverging, conventional focused, and coherent compounding method with $N = 9$ for the same interframe displacement of $384 \mu\text{m}$ at low myocardial velocities (Fig. 9) and 3.84 mm at high myocardial velocities (Fig. 10). At low myocardial velocities, the axial and lateral displacement, and strain images as well as the radial strain images, and correlation coefficient for coherent compounding method were of better quality than the ones obtained for the single diverging wave imaging and similar to those obtained with conventional focusing. At high myocardial velocities, with an interframe displacement of 3.84 mm , the three beamforming methods yielded poor displacement and strain estimation.

The axial, lateral, and radial strain estimation errors as well as the mean correlation coefficient are shown for each beamforming method at low and high myocardial velocities (Fig. 11). The quantitative analysis shows that at low

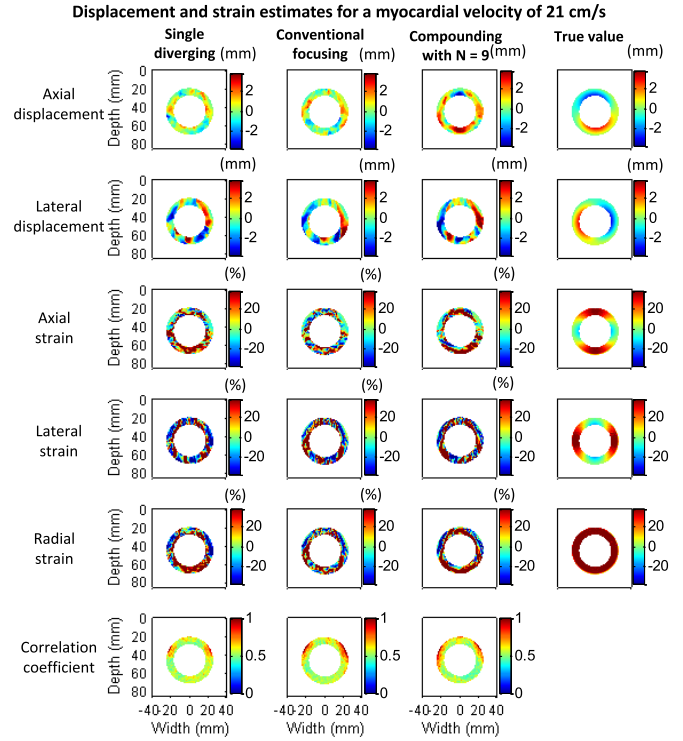


Fig. 10. Axial and lateral displacements and strains as well as radial strains and correlation coefficient in the phantom for single diverging wave imaging, conventional focusing, coherent compounding of $N = 9$ diverging waves and their true value, for an interframe displacement of 3.84 mm . The displacements and strains are poorly estimated for the three beamforming methods.

myocardial velocities, the axial, lateral, and radial strain estimation errors for coherent compounding with $N = 9$ are approximately similar to those obtained with conventional focusing and are significantly lower than for single diverging wave imaging. The axial strain estimation error is 19.9% for the single diverging method, 16.7% for the conventional focused method and 16.3% for coherent compounding with $N = 9$. The lateral strain estimation error is 80.3% for the single diverging method, 43.7% for the conventional focused method, and 40.4% for coherent compounding with $N = 9$. The radial strain estimation error is 30.6% for the single diverging method, 16% for the conventional focused method, and 18.9% for coherent compounding with $N = 9$. The mean correlation coefficient is 0.9516 for the single diverging method, 0.9846 for the conventional focused method, and 0.9821 for coherent compounding with $N = 9$. At high myocardial velocities, the mean correlation coefficient is 0.5707 for the single diverging method, 0.5716 for the conventional focused method, and 0.5510 for the coherent compounding with $N = 9$. For the three beamforming methods, the estimated strain ranges between 155.6% and 170.1% for axial, 359.7% and 451.6% for lateral, and 135.8% and 177.8% for radial.

C. In Vivo Feasibility

End systolic cumulative radial strains were estimated in a healthy volunteer using both the single diverging imaging sequence and the coherent compounding of $N = 9$ diverging

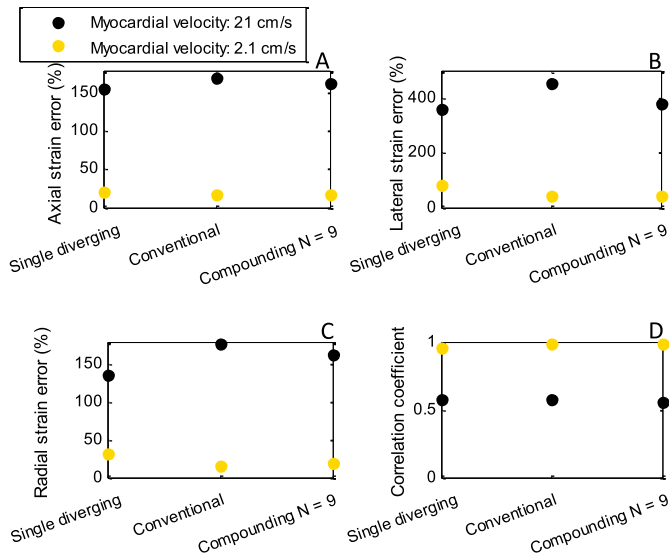


Fig. 11. (A) Axial, (B) lateral, and (C) radial strain error for single diverging wave imaging, conventional focusing, and coherent compounding of $N = 9$ diverging waves at low (2.1 cm/s) and high (21 cm/s) myocardial velocities. (D) Mean correlation coefficient inside the phantom is also shown.

waves (Fig. 12). Positive radial strains indicating radial thickening were mainly measured in the left ventricle and were more homogeneous for the compounding sequence compared to the single diverging one. Radial strains obtained with the compounding sequence were of better quality ($52.8 \pm 34.3\%$, $\text{SNRe} = 1.54$) than the ones obtained with the single diverging sequence ($62.5 \pm 50.5\%$, $\text{SNRe} = 1.24$).

IV. DISCUSSION

Previous studies have shown that cardiac strain imaging at high temporal resolution and during a single heart cycle can be achieved using single diverging wave imaging [3], [31]. However, this method suffers from stronger side lobes that can affect lateral displacement and strain estimation. Coherent compounding of diverging waves in the heart has been shown to improve SNR as well as the quality of tissue velocity images *in vivo*. However, the use of coherent compounding for cardiac strain imaging has not been investigated yet. The objective of this paper was to investigate the performance of coherent compounding of diverging waves in 2-D cardiac strain imaging.

A. PSF of Coherent Compounding

Initial investigation of the performance of coherent compounding of diverging waves was performed by obtaining the lateral PSF for each number of compounded waves. The level of the secondary lobes decreased as the number of compounded waves increased from 1 to 51, with a more rapid decrease between 1 and 9 compounded waves. This is consistent with previous studies showing the reduced effect of sidelobes when using coherent compounding of plane waves as opposed to a single plane wave [14], [15].

B. Performance of Coherent Compounding With Different Myocardial Velocities

A contracting heart in a short axis view was simulated as an annulus which inner radius decreased at

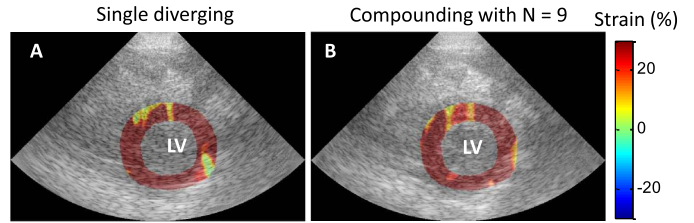


Fig. 12. Left ventricular (LV) end-systolic radial strain in a healthy volunteer using the (A) single diverging and the (B) coherent compounding sequence with $N = 9$. A noticeable improvement of radial strain, illustrated by a stronger homogeneity, (at 4 o'clock in A) is observed for the coherent compounded sequence compared to the single diverging one.

low (2.1 cm/s) or high (21 cm/s) velocities while the outer radius was kept constant. Cardiac strain imaging was performed with coherent compounding of diverging waves for the first time. Coherent compounding was performed with a number of diverging waves varying from 1 to 51 and a PRF of 7 kHz. Estimated axial and lateral displacements and strains were compared to their true value. As the number of diverging waves increased, the accuracy of the displacement and strain estimation as well as the correlation coefficient had a different behavior depending on the myocardial velocity.

1) *Null Myocardial Velocity:* The intrinsic effect of coherent compounding on displacement and strain estimation was investigated by not moving the phantom between diverging waves. A consistent increase in strain estimation accuracy and correlation coefficient was observed as the number of diverging waves increased. The radial strain error was closer to the axial strain error than to the lateral strain error. During radial contraction, lateral regions of the phantom have low axial displacements whereas top and bottom regions have higher axial displacement, and vice-versa for lateral displacements. Regions with very little or no displacement are better estimated axially than laterally, due to a higher axial sampling and resolution compared than for lateral. On the other hand, radial deformation is homogeneous and there is no region with little or no radial displacement. Therefore, radial deformation is better estimated and with an accuracy closer to the axial one. This increase was substantial from 1 to 9 diverging waves, while it was minor from 9 to 51 diverging waves, in agreement with a more significant reduction of sides lobes between 1 and 9 diverging waves as shown by the lateral PSF. Similar trends have been observed in the contrast [14], [32] and SNR [12] of echographic images while increasing the number of compounded waves.

2) *Low Myocardial Velocity:* A similar behavior of strain estimation accuracy was obtained at low myocardial velocities. However, the decrease in strain estimation error as a function of the number of diverging waves compounded was also caused by an increase in the interframe displacement due to motion between pulses. This was supported by the decrease in strain estimation error as the interframe displacement increases with single diverging wave imaging. Indeed, at very low interframe displacements, estimation errors can occur due to electronic noise, as illustrated by the Cramér–Rao lower bound [28] and to interpolation of the cross correlation function [33]. However, for a given interframe displacement,

the use of coherent compounding yielded strain errors lower than with single diverging wave imaging. The correlation coefficient increased from $N = 1$ to 9 and then decreased slightly. This behavior was influenced both by the interframe displacement and by coherent compounding. For a low interframe displacement, the benefit of coherent compounding seemed to increase sufficiently the SNR so that the correlation improves as the interframe displacement increases.

3) *High Myocardial Velocity*: The aforementioned benefit was, however, lost for higher interframe displacements due to higher decorrelation. In addition, motion between the first and the last frame in the compounding acquisition may impact the coherence of the summation of the RF signals, as it has been shown in previous studies [20], [34], [35]. This effect is more pronounced at high myocardial velocities. At a myocardial velocity of 21 cm/s, the axial, lateral and radial strain errors increased significantly when the number of compounded frames increases above approximately $N = 9$ to 15. This means that at a PRF of 7 kHz and a myocardial velocity of 21 cm/s, it is beneficial to compound up to approximately $N = 9$ to 15 consecutive RF frames, beyond this number, interframe displacements and strains are too large to estimate strain accurately. This is illustrated by the significant decrease in correlation coefficient as the number of compounded wave increases. This effect is supported by the increase in strain estimation error for an interframe displacement higher than approximately $600 \mu\text{m}$ ($\sim 1\lambda$), corresponding to an interframe radial strain of 6%, using single diverging wave imaging. Using coherent compounding decreases strain error, especially in the lateral direction, below an interframe displacement of approximately $600 \mu\text{m}$. For larger interframe displacements and strain, the addition of a higher number of diverging waves at high myocardial velocities without compensating the motion between frames worsen the displacement and strain estimation. Also, the motion between consecutive pulses at high myocardial velocities impacts the coherence of the summation of the RF signals to be compounded. *Denarie et. al.* [34] reported that a displacement larger than half a wavelength between frames yield significant loss in SNR and contrast in the compounded image. Therefore, using approximately $N = 9$ to 15 compounded waves appears to be a good compromise at both low and high myocardial velocities. A recent study has shown that it is possible to incorporate motion compensation to coherent compounding in order to reduce the effect of motion between compounded frames on contrast and tissue Doppler velocity estimation [20]. However, the performance of motion compensation for cardiac strain estimation with coherent compounding remains to be determined. Regardless, the number of transmits used to reconstruct one image should be limited to avoid significant decorrelation as well as poor motion and strain estimation between consecutive frames.

C. Effect of SNR and Background Medium Level

As shown in Fig. 5, an SNR inferior to 15 dB or a scattering amplitude ratio inferior to 5, which can be obtained for low contrast images, is associated with more radial strain estimation errors with $N = 9$ compounded waves. On the

other hand, for a SNR superior to 15 dB and a scattering amplitude ratio superior to 5, the radial strain accuracy reaches a plateau. Therefore, the strain estimation accuracy can be impacted if the SNR or the contrast is too poor, but the number of diverging waves can be adjusted to reduce this effect, as long as it does not induce significant decorrelation, which can be up to 9 to 15 diverging waves with the imaging parameters used in this study.

D. Comparison of Different Beamforming Methods

The comparison between the different beamforming techniques also showed that at low myocardial velocities, coherent compounding always performed better than single diverging wave imaging for the same interframe displacement. This corroborates what was observed when comparing the results between $N = 1$ and $N = 9$, except, in this case, the full aperture is used in transmit for the single diverging wave. Coherent compounding with $N = 9$ provided strain estimation in the same order of that obtained with conventional focused waves. At high myocardial velocities, the displacement and strain were poorly estimated in the simulated configuration. Indeed, for conventional focusing, 128 lines were beamformed; therefore, at a myocardial velocity of 21 cm/s and a PRF of 7 kHz, the interframe displacement of the inner boundary of the annulus would be 3.84 mm ($\sim 6.2\lambda$), corresponding to an interframe strain of 38.4%. This interframe displacement and strain were too large for the motion to be accurately estimated using our RF tracking method, as indicated by the correlation coefficient (~ 0.5). However, 2-D speckle tracking of cardiac B-mode images with conventional imaging is feasible, but uses a different tracking method from the one presented in this paper [36], [37]. In addition, physiological myocardial velocities may not be always as high as 21 cm/s and the number of beams can be reduced to decrease the interframe displacement and strain so that it could more accurately be estimated.

E. In Vivo Feasibility

The simulation results were confirmed by the *in vivo* feasibility experiment. The use of $N = 9$ compounded diverging waves provided better strain estimation than using a single diverging wave in a healthy volunteer (Fig. 12). In some regions, lower radial strains were found for both single diverging wave imaging and coherent compounding, while relatively homogeneous radial strain is expected in the entire cross section since it was a normal heart. However, fewer regions with low radial strain were found with coherent compounding than with single diverging wave imaging, indicating better estimation for the former method. *In vivo* comparison was not performed with conventional imaging in this study, due to a lower frame rate (~ 50 Hz), which would entail larger interframe strain, and therefore, poorer RF tracking [38]. In future studies, the performance of this technique *in vivo* will be compared to that of the clinically used 2-D speckle tracking echocardiography. An improvement in cardiac strain estimation can have a deep impact on early detection of coronary artery disease (CAD) using ultrasound. A larger scale

study should be carried out in order to further investigate this initial feasibility as well as the potential of coherent compounding to detect and characterize CAD.

While significant findings, such as localizing pacing sites and characterizing bundle branch block activation in cardiac resynchronization therapy patients, were obtained with single diverging wave imaging to image cardiac strain at a high frame rate [31], the use of compounded waves is expected to improve the performance of cardiac strain-based diagnosis methods. In particular, Myocardial Elastography [29], which is used to detect and characterize contraction abnormalities in CAD patients and which relies both on axial and lateral displacement estimation, should significantly benefit from coherent compounding of diverging waves for high temporal resolution imaging during a single heartbeat.

F. Limitations

The results presented in the simulation study were obtained by modeling the left ventricle in short-axis view as a thickening and rotating annulus. One of the limitations of this study is that the heart has a 3-D geometry and moves in all three directions of space. However, the majority of echocardiography in the clinic is performed with 2-D ultrasound scan. Nevertheless, an annulus is a rough approximation of the true geometry of the left ventricle in short-axis view, and the radial thickening of the myocardium during systole may not be as homogeneous as modeled in this study. In addition, out-of-plane motion was not modeled in this study and may increase decorrelation of RF signals, and therefore decrease the accuracy of displacement and strain estimation. High frame rate 3-D echocardiography has recently been shown *in vivo* [32] and could be used to estimate elevational motion, in addition to axial and lateral ones, in order to limit decorrelation and estimate 3-D cardiac strain in the total volume of the heart.

Ultrasound attenuation in tissue due to absorption was not taken into account in this study and can also decrease the accuracy of displacement and strain estimation especially at larger depths. *In vivo* experimental conditions such as the presence of ribs can also produce acoustic shadowing artifacts and affect the accuracy of displacement and strain estimation. Despite the limitations of the model presented in this study with regard to *in vivo* echocardiography, they are independent of the beamforming method, and therefore, the intrinsic performance of coherent compounding of diverging waves could be compared to that of single diverging wave imaging irrespective of these limitations. In addition, simulations constitute an ideal framework as a first step to investigate the performance of a method where the true value of a quantity to be estimated is known. As mentioned previously, the trend in the improvement of strain estimation as a function of the number of compounded waves at low myocardial velocities is similar to what has been observed experimentally with the contrast and SNR of echographic images. Future studies will include a larger number of subjects to investigate the performance of coherent compounding for cardiac strain imaging and in particular for characterizing CAD.

V. CONCLUSION

In this paper, coherent compounding was used for the first time to image cardiac strain. The accuracy and performance of displacements and strain estimation increased significantly with the number of compounded waves. Nine to fifteen compounded diverging waves constituted a good compromise at both low and high myocardial velocities regarding strain estimation quality. Initial feasibility of imaging cardiac strain with coherent compounding was shown in a healthy volunteer. These results are very promising for high frame rate cardiac strain-based diagnosis methods. Ongoing *in vivo* studies are under investigation to assess the performance of this technique in healthy subjects and CAD patients.

REFERENCES

- [1] W.-N. Lee, J. Provost, K. Fujikura, J. Wang, and E. E. Konofagou, "In vivo study of myocardial elastography under graded ischemia conditions," *Phys. Med. Biol.*, vol. 56, no. 4, pp. 1155–1172, Feb. 2011.
- [2] F. J. van Slochteren *et al.*, "Layer-specific radiofrequency ultrasound-based strain analysis in a porcine model of ischemic cardiomyopathy validated by a geometric model," *Ultrasound Med. Biol.*, vol. 40, pp. 378–388, Feb. 2014.
- [3] E. A. Bunting, J. Provost, and E. E. Konofagou, "Stochastic precision analysis of 2D cardiac strain estimation *in vivo*," *Phys. Med. Biol.*, vol. 59, no. 22, pp. 6841–6858, Nov. 2014.
- [4] D. P. Shattuck, M. D. Weinschenker, S. W. Smith, and O. T. von Ramm, "Explososcan: A parallel processing technique for high speed ultrasound imaging with linear phased arrays," *J. Acoust. Soc. Amer.*, vol. 75, no. 4, pp. 1273–1282, Apr. 1984.
- [5] M. V. Andersen *et al.*, "High-frame-rate deformation imaging in two dimensions using continuous speckle-feature tracking," *Ultrasound Med. Biol.*, vol. 42, no. 11, pp. 2606–2615, Nov. 2016.
- [6] L. Tong, A. Ramalli, R. Jasaityte, P. Tortoli, and J. D'Hooge, "Multi-transmit beam forming for fast cardiac imaging—Experimental validation and *in vivo* application," *IEEE Trans. Med. Imag.*, vol. 33, no. 6, pp. 1205–1219, Jun. 2014.
- [7] L. Tong *et al.*, "Wide-angle tissue Doppler imaging at high frame rate using multi-line transmit beamforming: An experimental validation *in vivo*," *IEEE Trans. Med. Imag.*, vol. 35, no. 2, pp. 521–528, Feb. 2016.
- [8] S. Wang, W.-N. Lee, J. Provost, J. Luo, and E. E. Konofagou, "A composite high-frame-rate system for clinical cardiovascular imaging," *IEEE Trans. Ultrason., Ferroelect., Freq. Control*, vol. 55, no. 10, pp. 2221–2233, Oct. 2008.
- [9] L. Sandrin, S. Catheline, M. Tanter, X. Hennequin, and M. Fink, "Time-resolved pulsed elastography with ultrafast ultrasonic imaging," *Ultrason. Imag.*, vol. 21, no. 4, pp. 259–272, Oct. 1999.
- [10] M. Cikes, L. Tong, G. R. Sutherland, and J. D'Hooge, "Ultrafast cardiac ultrasound imaging: Technical principles, applications, and clinical benefits," *JACC Cardiovascular Imag.*, vol. 7, no. 8, pp. 812–823, Aug. 2014.
- [11] H. Hasegawa and H. Kanai, "High-frame-rate echocardiography with reduced sidelobe level," *IEEE Trans. Ultrason., Ferroelect., Freq. Control*, vol. 59, no. 11, pp. 2569–2575, Nov. 2012.
- [12] C. Papadacci, M. Pernot, M. Couade, M. Fink, and M. Tanter, "High-contrast ultrafast imaging of the heart," *IEEE Trans. Ultrason., Ferroelect., Freq. Control*, vol. 61, no. 2, pp. 288–301, Feb. 2014.
- [13] J. Provost *et al.*, "Electromechanical wave imaging for arrhythmias," *Phys. Med. Biol.*, vol. 56, no. 22, pp. L1–L11, Nov. 2011.
- [14] G. Montaldo, M. Tanter, J. Bercoff, N. Benech, and M. Fink, "Coherent plane-wave compounding for very high frame rate ultrasonography and transient elastography," *IEEE Trans. Ultrason., Ferroelect., Freq. Control*, vol. 56, no. 3, pp. 489–506, Mar. 2009.
- [15] S. Korukonda, R. Nayak, N. Carson, G. Schifitto, V. Dogra, and M. M. Doyley, "Noninvasive vascular elastography using plane-wave and sparse-array imaging," *IEEE Trans. Ultrason., Ferroelect., Freq. Control*, vol. 60, no. 2, pp. 332–342, Feb. 2013.
- [16] J. Porée, D. Garcia, B. Chayer, J. Ohayonm, and G. Cloutier, "Noninvasive vascular elastography with plane strain incompressibility assumption using ultrafast coherent compound plane wave imaging," *IEEE Trans. Med. Imag.*, vol. 34, no. 12, pp. 2618–2631, Dec. 2015.
- [17] R. S. C. Cobbold, *Fundations of Biomedical Ultrasound*. London, U.K.: Oxford Univ. Press, 2007.

- [18] M. Karaman, P.-C. Li, and M. O'Donnell, "Synthetic aperture imaging for small scale systems," *IEEE Trans. Ultrason., Ferroelectr., Freq. Control*, vol. 42, no. 3, pp. 429–442, May 1995.
- [19] M. M. Nillesen *et al.*, "Cardiac motion estimation using ultrafast ultrasound imaging tested in a finite element model of cardiac mechanics," in *Proc. 8th Int. Conf. Funct. Imag. Modeling Heart (FIMH)*, Jun. 2015, pp. 207–214.
- [20] J. Poree, D. Posada, A. Hodzic, F. Tournoux, G. Cloutier, and D. Garcia, "High-frame-rate echocardiography using coherent compounding with Doppler-based motion-compensation," *IEEE Trans. Med. Imag.*, vol. 35, no. 7, pp. 1647–1657, Jul. 2016.
- [21] P. Baraldi, A. Sarti, C. Lamberti, A. Prandini, and F. Sgallari, "Evaluation of differential optical flow techniques on synthesized echo images," *IEEE Trans. Biomed. Eng.*, vol. 43, no. 3, pp. 259–272, Mar. 1996.
- [22] M. Suhling, M. Arigovindan, C. Jansen, P. Hunziker, and M. Unser, "Myocardial motion analysis from B-mode echocardiograms," *IEEE Trans. Image. Process.*, vol. 14, no. 4, pp. 525–536, Apr. 2005.
- [23] R. M. Lang *et al.*, "Recommendations for chamber quantification," *Eur. J. Echocardiogr.*, vol. 7, no. 2, pp. 79–108, Mar. 2006.
- [24] H. Dalen, A. Thorstensen, L. J. Vatten, S. A. Aase, and A. Stoylen, "Reference values and distribution of conventional echocardiographic Doppler measures and longitudinal tissue Doppler velocities in a population free from cardiovascular disease," *Circulat., Cardiovascular Imag.*, vol. 10, no. 5, pp. 614–622, Sep. 2010.
- [25] H.-K. Kim *et al.*, "Assessment of left ventricular rotation and torsion with two-dimensional speckle tracking echocardiography," *J. Amer. Soc. Echocardiogr.*, vol. 20, no. 1, pp. 45–53, Jan. 2007.
- [26] J. A. Jensen, "Field: A program for simulating ultrasound systems," in *Proc. Med. Biol. Eng. Comput.*, vol. 4, 1996, pp. 351–353.
- [27] J. A. Jensen and S. I. Nikolov, "Fast simulation of ultrasound images," in *Proc. IEEE Ultrason. Symp.*, vol. 2, Oct. 2000, pp. 1721–1724.
- [28] T. Varghese and J. Ophir, "A theoretical framework for performance characterization of elastography: The strain filter," *IEEE Trans. Ultrason., Ferroelect., Freq. Control*, vol. 44, no. 1, pp. 164–172, Jan. 1997.
- [29] W.-N. Lee, C. M. Ingrassia, S. D. Fung-Kee-Fung, K. D. Costa, J. W. Holmes, and E. E. Konofagou, "Theoretical quality assessment of myocardial elastography with *in vivo* validation," *IEEE Trans. Ultrason., Ferroelect., Freq. Control*, vol. 54, no. 11, pp. 2233–2245, Nov. 2007.
- [30] J. Luo, J. Bai, P. He, and K. Ying, "Axial strain calculation using a low-pass digital differentiator in ultrasound elastography," *IEEE Trans. Ultrason., Ferroelect., Freq. Control*, vol. 51, no. 9, pp. 1119–1127, Sep. 2004.
- [31] J. Provost, A. Gambhir, J. Vest, H. Garan, and E. E. Konofagou, "A clinical feasibility study of atrial and ventricular electromechanical wave imaging," *Heart Rhythm*, vol. 10, pp. 856–862, Jun. 2013.
- [32] J. Provost *et al.*, "3D ultrafast ultrasound imaging *in vivo*," *Phys. Med. Biol.*, vol. 59, no. 19, pp. L1–L13, Oct. 2014.
- [33] I. Céspedes, Y. Huang, J. Ophir, and S. Spratt, "Methods for estimation of subsample time delays of digitized echo signals," *Ultrason. Imag.*, vol. 17, no. 2, pp. 142–171, Apr. 1995.
- [34] B. Denarie *et al.*, "Coherent plane wave compounding for very high frame rate ultrasonography of rapidly moving targets," *IEEE Trans. Med. Imag.*, vol. 32, no. 7, pp. 1265–1276, Jul. 2013.
- [35] K. L. Gammelmark and J. A. Jensen, "2-D tissue motion compensation of synthetic transmit aperture images," *IEEE Trans. Ultrason., Ferroelect., Freq. Control*, vol. 61, no. 4, pp. 594–610, Apr. 2014.
- [36] U. Adamu, F. Schmitz, M. Becker, M. Kelm, and R. Hoffmann, "Advanced speckle tracking echocardiography allowing a three-myocardial layer-specific analysis of deformation parameters," *Eur. J. Echocardiogr.*, vol. 10, no. 2, pp. 303–308, Mar. 2009.
- [37] J. Gorcsan, III, and H. Tanaka, "Echocardiographic assessment of myocardial strain," *J. Amer. College Cardiol.*, vol. 58, no. 14, pp. 1401–1413, Sep. 2011.
- [38] T. Varghese and J. Ophir, "Characterization of elastographic noise using the envelope of echo signals," *Ultrasound Med. Biol.*, vol. 24, no. 4, pp. 543–555, May 1998.



Julien Grondin was born in Saint-Denis, Reunion Island, France, in 1983. He received the M.S. degree from Paris Diderot University (University of Paris VII), Paris, France, in 2007, and the Ph.D. degree from Pierre and Marie Curie University (University of Paris VI), Paris, in 2010.

In 2011, he joined the Ultrasound and Elasticity Imaging Laboratory as a Post-Doctoral Research Scientist, and is currently an Associate Research Scientist with the Department of Biomedical Engineering, Columbia University, New York, NY, USA.

His research interests included ultrasonic characterization of bone properties. His current research interests include cardiac ultrasound imaging, myocardial elastography, and high-intensity focused ultrasound ablation monitoring.



Vincent Sayseng received the B.S. degree in biomedical engineering from the University of Rochester, NY, USA, in 2014. Since 2014, he has been a Biomedical Engineering Student in the M.S./Ph.D. program with Columbia University, New York, NY, USA.

His current research interests include ultrasound imaging to characterize the electrical and mechanical behavior of the heart in a noninvasive fashion.



Elisa E. Konofagou (S'98–A'99–M'03) is the Robert and Margaret Hariri Professor of Biomedical Engineering and Professor of Radiology as well as the Director of the Ultrasound and Elasticity Imaging Laboratory at the Biomedical Engineering department of Columbia University, New York, NY, USA. She has coauthored over 170 articles. Her research interests include the development of novel elasticity imaging techniques and therapeutic ultrasound methods and more notably, myocardial elastography, electromechanical and pulse wave imaging, harmonic motion imaging, focused ultrasound therapy, and drug delivery in the brain, with several clinical collaborations in the Columbia Presbyterian Medical Center and elsewhere.

Prof. Konofagou is also a Technical Committee Member of the Acoustical Society of America, the International Society of Therapeutic Ultrasound, the IEEE Engineering in Medicine and Biology conference, the IEEE International Ultrasonics Symposium, and the American Association of Physicists in Medicine. She serves as an Associate Editor in the journals of IEEE TRANSACTIONS ON ULTRASONICS, FERROELECTRICS, AND FREQUENCY CONTROL, *Ultrasonic Imaging and Medical Physics*, and is a recipient of awards such as the CAREER award by the National Science Foundation (NSF) and the Nagy award by the National Institutes of Health (NIH) as well as others by the American Heart Association, the Acoustical Society of America, the American Institute of Ultrasound in Medicine, the Wallace H. Coulter Foundation, the Bodossaki Foundation, the Society of Photo-optical Instrumentation Engineers (SPIE), and the Radiological Society of North America (RSNA).